Bakker A., Oshinowo L.M. (2004). Modelling of Turbulence in Stirred Vessels Using Large Eddy Simulation. Trans IChemE Vol. 82 Issue A9 Special issue: In Honour of Professor Alvin W. Nienow. September 2004. pp. 1169-1178.

IChemE

www.ingentaselect.com/titles/02638762.htm

0263–8762/04/$30.00+0.00

Trans IChemE, Part A, September 2004

MODELLING OF TURBULENCE IN STIRRED VESSELS USING LARGE EDDY SIMULATION

A. BAKKER[1,*] and L. OSHINOWO[2]

[1]*Fluent, Inc., Lebanon, NH, USA*
[2]*Hatch, Mississauga, Ontario, Canada*

The application of large eddy simulation (LES) to the prediction of large-scale chaotic structures in stirred tanks is investigated. Typical stirrer configurations representing different flow regimes are assessed: a single radial pumping impeller, single axial pumping impellers, multiple hydrofoil impellers, and a retreat curve impeller. The dynamic turbulent flow field in each configuration is calculated using LES. The impeller motion is explicitly modelled using the sliding mesh model. It is concluded that the flow fields in stirred vessels are very rich in structure and that a wide variety of flow regimes exist. The predicted flow patterns compare well with digital particle image velocimetry data reported in the literature, and exhibit the long time-scale instabilities seen in experiments reported in the literature.

Keywords: large eddy simulation (LES); mixing; turbulence; computational fluid dynamics (CFD).

INTRODUCTION

Prediction of mixing of multi-component fluids is important in many chemical process applications. Although laminar mixing is a complicated process per se, there is a far greater challenge in predicting the mixing in turbulent flows because of the intrinsically chaotic nature of turbulent flows. In turbulent flows, large-scale eddies with coherent structures are mainly responsible for the mixing of passive scalars. The large-scale eddies embody themselves in the form of identifiable and organized distributions of vorticity.

Experimental work suggests that large-scale, time-dependent structures, with periods much longer than the time of an impeller revolution, are involved in many of the fundamental hydrodynamic processes in stirred vessels. For example, local velocity data histograms may be bimodal or trimodal, even though they are usually analysed as having only one mode in most laser Doppler experiments (Bakker and Van den Akker, 1994a). The gas holdup distribution may be asymmetric and oscillating (Bakker and Van den Akker, 1994b). In solids suspension processes, solids can be swept from one side of the vessel to the other in a relatively slow oscillating pattern, even in dilute suspensions. Digital particle image velocimetry experiments have shown that large-scale asymmetries with periods up to several minutes exist in stirred vessels equipped with axial flow impellers (Myers *et al.*, 1997).

*Correspondence to: Dr A. Bakker, Fluent, Inc., 10 Cavendish Court, Lebanon, NH 03766, USA.
E-mail: ab@fluent.com

In this study, the application of large eddy simulation (LES) to the prediction of these large-scale chaotic structures in stirred tanks is investigated. Various flow regimes produced by typical stirrer configurations were assessed: a single radial pumping impeller, a single axial pumping pitched blade turbine, a single high-efficiency impeller, a multiple impeller system, and a retreat curve impeller (RCI) with partial baffling. The impeller rotation was modelled using a sliding mesh model on unstructured grids using the finite volume method (Mathur, 1994; Bakker *et al.*, 1997).

Previous LES results reported in the literature include work using the lattice-Boltzmann method by Eggels (1996), Derksen and Van den Akker (1999), and Hartmann *et al.* (2003). Studies using the finite volume method include work by Roussinova (2001) and Yeoh *et al.* (2003). The current work differs from these previously reported studies in that a wider range of flow regimes is analysed.

The theory behind LES, the model, and the results will be discussed. [Note: this article is based on material presented at the 10th European Conference on Mixing (Bakker *et al.*, 2000), and additional material from oral presentations at MIXING XVIII (Bakker *et al.*, 2001) and CHISA 2002 (Bakker *et al.*, 2002).]

THEORETICAL

The LES Model

The numerical modelling of these complicated mixing processes is a daunting task. Direct numerical simulation (DNS) provides the most exact approach in which the mechanism involved in turbulent mixing can be accurately

represented. It requires resolving the smallest eddies, which makes the approach prohibitively expensive even with the most powerful computers of the present day, and for the foreseeable future too.

On the other hand, the popular approaches based on the Reynolds-averaged Navier–Stokes (RANS) equations amount to averaging out the large eddies that are mainly responsible for mixing. One is left to model the effects of large eddies by relying on empirical data and phenomenological reasoning and hypotheses. The RANS approach is computationally efficient, and provides useful engineering data such as impeller torque, macroscopic flow patterns, and is relatively easily extended to multiphase flow and chemical reaction simulations.

Recently, the LES approach has been used as an intermediate method between the extremes of DNS and RANS. The premise underlying LES is that any turbulent flow consists of eddies, and involves a wide spectrum of scale. In LES, large eddies are resolved directly, and small eddies are modelled. The rationale behind LES can be summarized as follows. Momentum, mass, energy, and other passive scalars are transferred mostly by large eddies. Large eddies are more dependent on the geometries and boundary conditions of the flow involved, and are highly anisotropic. Small eddies are less dependent on the geometry, and tend to be more isotropic, and consequently are more universal. The chance of finding a universal model is much higher when only small eddies are modelled. In LES, the governing equations are obtained by spatially filtering the Navier–Stokes equations. The large turbulent scales are computed explicitly, while the small scales are modelled using one of a number of available subgrid scale (SGS) models. The SGS models describe interactions between the resolved and unresolved scales. The LES is more general than the RANS approach, and avoids the RANS dependence on boundary conditions for the large-scale eddies. Like DNS, LES gives a three-dimensional, time-dependent solution. The required computational resources for LES are between those of DNS (10 to 1000 times less) and RANS (10 to 100 times more). The LES model can be used at much higher Reynolds numbers than DNS because the computational effort is independent of the Reynolds number if the small scales obey the inertial range spectrum and the near-wall effects are not important.

Governing Equations

The governing equations for LES are obtained by spatially filtering over small scales. Filtering eliminates the eddies whose scales are smaller than the filter width. In the current study, a top-hat filter of filter width to grid size ratio of two is used. Explicit filtering is not used since with this filter, differentiation and filtering operations commute only on uniform grids. The importance of commutation errors on non-uniform grids is a topic of current research. In the present work, it is assumed that the commutation error is a part of the error in the subgrid models. Applying the filtering operation to the momentum equation, we obtain

$$\frac{\partial \bar{\rho}\tilde{u}_i}{\partial t} + \frac{\partial \bar{\rho}\tilde{u}_i\tilde{u}_j}{\partial x_j} = -\frac{\partial \bar{p}}{\partial x_i} + \frac{\partial \bar{\tau}_{ij}}{\partial x_j} + \frac{\partial \sigma_{ij}}{\partial x_j} \tag{1}$$

where $\tilde{u}_i$ is the filtered velocity and $\bar{\tau}_{ij}$ is the filtered shear stress tensor. In the filtered equations, the terms represented by σ_{ij}, called the SGS stresses/fluxes, are of the form

$$\sigma_{ij} = -(\overline{\rho u_i u_j} - \bar{\rho}\tilde{u}_i\tilde{u}_j) \tag{2}$$

These SGS stresses/fluxes are unknown, and need to be modelled. Smagorinsky (1963) and Lilly (1966) developed the most basic subgrid scale model. In this model, the turbulent viscosity is modelled by

$$\mu_t = \rho L_s^2 |\bar{S}| \tag{3}$$

where L_s is the mixing length for subgrid scales, and $|\bar{S}| = \sqrt{(2\bar{S}_{ij}\bar{S}_{ij})}$, where $\bar{S}_{ij}$ is the rate of strain tensor for the resolved scales. The mixing length is computed in FLUENT as $\mu L_s = \min(\kappa d, C_s V^{1/3})$ where κ and C_s are constants, d is the distance to the closest wall, and V is the volume of the cell.

Yakhot *et al.* (1986) have obtained an RNG subgrid scale stress model by performing recursive elimination of infinitesimal bands of small scales. In the RNG SGS model, subgrid fluxes in the momentum equation are represented by

$$\sigma_{ij} - \frac{1}{3}\sigma_{kk}\delta_{ij} = 2\mu_{sgs}\bar{S}_{ij} \tag{4}$$

The RNG subgrid model differs from the Smagorinsky model in that the effective viscosity, $\mu_{eff} = \mu + \mu_t$, is given by

$$\mu_{eff} = \mu\left[1 + H\left(\frac{\mu_{sgs}^2\mu_{eff}}{\mu^3} - C\right)\right]^{1/3} \tag{5}$$

where $\mu_{sgs} = \bar{\rho}(C_{rng}\sqrt[3]{V})^2(2\bar{S}_{ij}\bar{S}_{ij})^{1/2}$ and $H(x)$ is the Heaviside step function. The coefficients, $C_{rng} = 0.157$ and $C = 100$ are obtained from the theory.

In highly turbulent regions, the filtering operation results in a very high subgrid viscosity compared to the molecular viscosity, $\mu_{sgs} \gg \mu$ and $\mu_{eff} \cong \mu_{sgs}$. In this limit, the RNG theory based subgrid scale model returns to the Smagorinsky model with a different model constant. In weakly turbulent regions, the argument of the Heaviside function is negative, and the effective viscosity is equal to the molecular viscosity. The RNG SGS model in this limit correctly yields zero SGS viscosity in low Reynolds number flows without any ad hoc modifications. All simulations reported in this paper used the RNG subgrid model.

Numerical Method

The numerical simulations are conducted using FLUENT. A detailed discussion of the numerical method and several validation studies of this code are given by Murthy and Mathur (1998). In this code, the domain is

discretized into arbitrary unstructured polyhedra. The discretized form of the governing equations for each cell is obtained such that the conservation principles are obeyed on each polyhedron. In FLUENT, the linear equations are solved using an algebraic multigrid procedure. The results presented in this paper are obtained using central differencing for spatial discretization of the momentum equations, and time-advancement via a second-order accurate implicit scheme. The transient impeller motion was modelled using the sliding mesh model for unstructured grids (Mathur, 1994).

MODEL DESCRIPTION

The modelling results of the transient, turbulent hydrodynamics are reported below for five configurations studied.

The first configuration is a 45° pitched-blade turbine (PBT) configuration consisting of a cylindrical, flat-bottomed tank of internal diameter $T = 292$ mm, with four full-length baffles of width $T/12$. The free surface is at a height $H = T$. The PBT has four blades, with a diameter $D = 0.35T$, a blade width $W = 0.20D$, and a blade thickness of 1 mm. The impeller centre is positioned at a distance $C = 0.46T$ off the tank bottom. The impeller is mounted on a 10 mm diameter shaft rotating at 60 rpm. The impeller Reynolds number was 1.0×10^4. This geometry was studied experimentally by Myers *et al.* (1997). The computational grid was defined by 527,000 unstructured, non-uniformly distributed, hexahedral cells. In total, 178 s of actual time, covering 178 revolutions, were simulated, starting from a zero-velocity flow field. A time step of 0.01 s was used, which corresponds to 100 time steps per impeller revolution.

The second configuration consists of a single Rushton impeller in a cylindrical, flat-bottomed tank of internal diameter, $T = 202$ mm, with four full-length baffles of width 22 mm. The free surface is at a height, $H = T$. The impeller has a diameter $D = T/3$, a blade width $W = 0.20D$ and a blade thickness of 1 mm. The impeller centre is positioned at a distance $C = T/3$ off the tank bottom. The impeller is mounted on a 5 mm diameter shaft rotating at 290 rpm. The impeller Reynolds number was 2.2×10^4. The computational grid was defined by 763,000 unstructured, non-uniformly distributed, hexahedral cells. Approximately 4.6 s of actual time were simulated. This covers 22 revolutions, starting from a flow field calculated using a steady-state RANS model. A time step of 0.00345 s was used, which corresponds to 60 time steps per impeller revolution.

A system with a single three-blade high-efficiency impeller was the third configuration studied. The simulations were performed for a flat bottom vessel with four baffles. The vessel diameter is $T = 0.292$ m. The liquid level is equal to the tank diameter, $Z/T = 1$. The liquid is water. The impeller is a Chemineer HE-3 with a D/T of 0.39 and an off bottom clearance of $C/T = 0.33$. The impeller speed is 60 rpm and the impeller Reynolds number is approximately 1.3×10^4. This same system was studied experimentally by Myers *et al.* (1997). An unstructured hexahedral mesh with approximately 500,000 cells was used. In total, 46 s of actual time were simulated. This covers 46 revolutions, starting from a flow field calculated using a steady-state RANS model. A time step of 0.00923 s was used, which corresponds to 108 time steps per impeller revolution.

The fourth configuration was a vessel equipped with four A310 impellers. The vessel diameter is 0.232 m. The liquid level is 0.944 m ($Z/T = 4$). The impeller diameter is 0.097 m ($D/T = 0.42$) for all impellers. The distance between the impellers is 0.236 m. The lower impeller is located 0.118 m above the vessel bottom. The liquid is water. The vessel is closed with a flat lid on top. The vessel is equipped with four baffles with $W_b/T = 0.1$. The baffles are attached to the wall. The impeller speed was 300 rpm. The impeller Reynolds number was 4.7×10^4. An unstructured hexahedral mesh with approximately 500,000 cells was used. In total, 23.6 s of actual time were simulated. This covers 118 revolutions, starting from a flow field calculated using a steady-state RANS model. A time step of 0.005 s was used, which corresponds to 40 time steps per impeller revolution.

The fifth, and final, configuration was a typical glass-lined vessel equipped with a retreat curve impeller (RCI). An eight cubic-metre vessel was used, filled with water to a level of 5.8 m^3. The impeller has a D/T of 0.49 and rotation speed of 180 rpm. The Reynolds number is on the order of 3×10^6. The vessel is equipped with a standard fin baffle and a diptube. A hybrid, unstructured mesh containing approximately 630,000 tetrahedral and hexahedral cells was used. In total, 10 s of actual time were simulated. This covers 30 revolutions, starting from a flow field calculated using a steady-state RANS model. A time step of 0.00556 s was used, which corresponds to 60 time steps per impeller revolution.

All computational grids were created such that the grid was finer in the impeller region than in the rest of the domain. In all cases the mesh was fine enough that eddies in the inertial subrange could be resolved. The first cell centre near the walls was inside the laminar sublayer in most of the domain for the two lowest Reynolds number cases: the PBT case and the HE-3 case. For the three highest Reynolds number cases (Rushton, four A310, RCI) the first cell center near the walls was in the logarithmic region of the boundary layer throughout the domain, and standard wall functions were used to calculate the wall shear stresses.

RESULTS

Flow Field Results for the PBT

Figure 1 shows velocity vector plots after 162, 166, 170, and 174 s, respectively, for the simulations with the pitched blade turbine. These vector plots show the unsteadiness in the flowfield. Figure 1a shows a relatively symmetric axial flow pattern. Figure 1b shows an asymmetric flow pattern, with the flow on the left side of the vessel being axial, and a jet originating from the impeller impinging on the vessel bottom. On the right side of the vessel, the jet emanating from the impeller follows a radial trajectory and attaches to the vessel wall. Figure 1c shows a flow pattern where the jet coming from the impeller attaches to the vessel wall on both sides, with a secondary circulation loop formed near the vessel bottom. Figure 1d shows a relatively

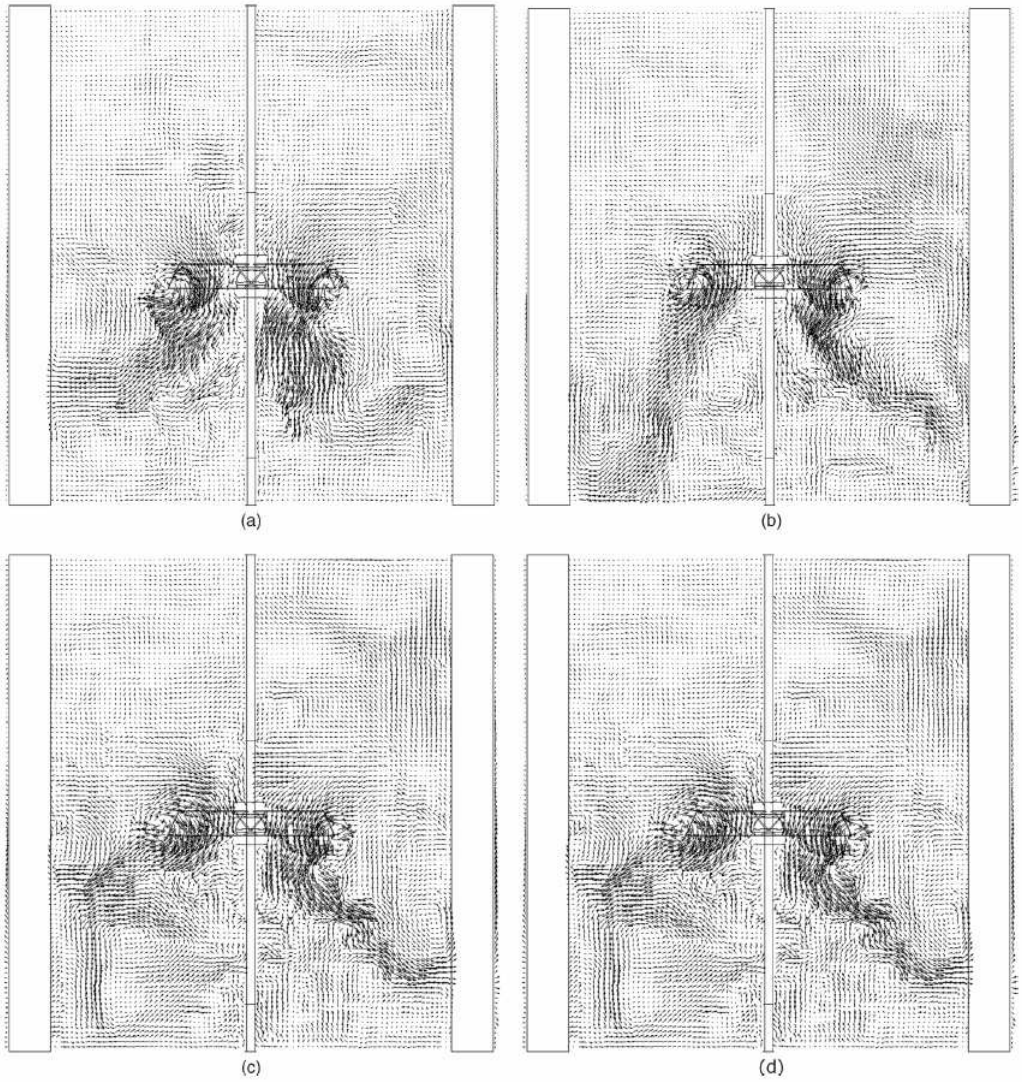

Figure 1. The pitched blade turbine flow pattern after (a) 162, (b) 166, (c) 170, and (d) 174 s.

symmetric flow pattern once again where the axial jet from the impeller attaches to the vessel bottom.

Qualitatively, these results compare strikingly well with the digital particle image velocimetry data reported by Myers *et al.* (1997). Their experimental data also showed the existence of these unsteady, asymmetric flow patterns.

Note that these flow pattern oscillations have a time-scale that is much longer than the time-scale associated with the impeller blade passage frequency. Figure 2 shows the simulated flow patterns at three instants in time, spaced apart by half a blade passage period, or 0.125 s. The overall flow pattern, which is asymmetric, does not change during this time. This also agrees with the experimental data reported by Myers *et al.* (1997).

Time Series Results for the PBT

Figure 3 shows time series of the axial velocity in four locations. A Cartesian reference frame is used with the origin being on the axis at the liquid surface, and x being the downward axial direction. Significant fluctuations can be observed, with the axial velocity periodically changing direction in certain locations. These time series also show that the period of the fluctuations is not constant. Higher frequency variations are observed in locations (b) and (c),

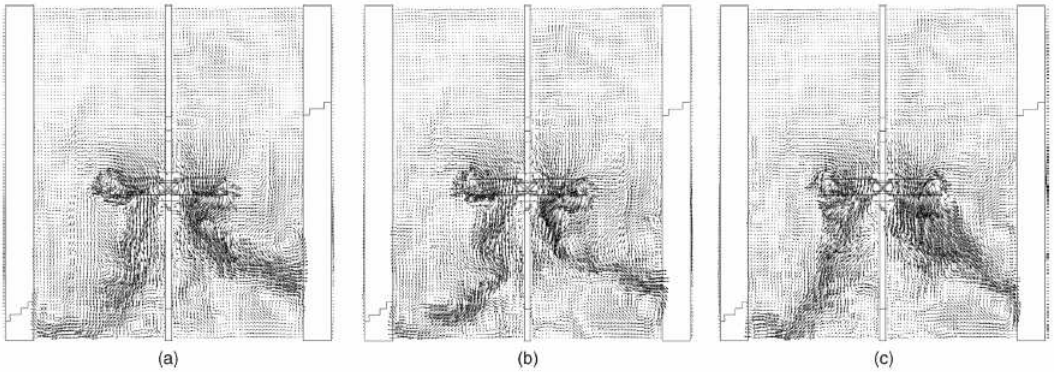

Figure 2. Instantaneous velocity fields of the PBT taken during blade passage.

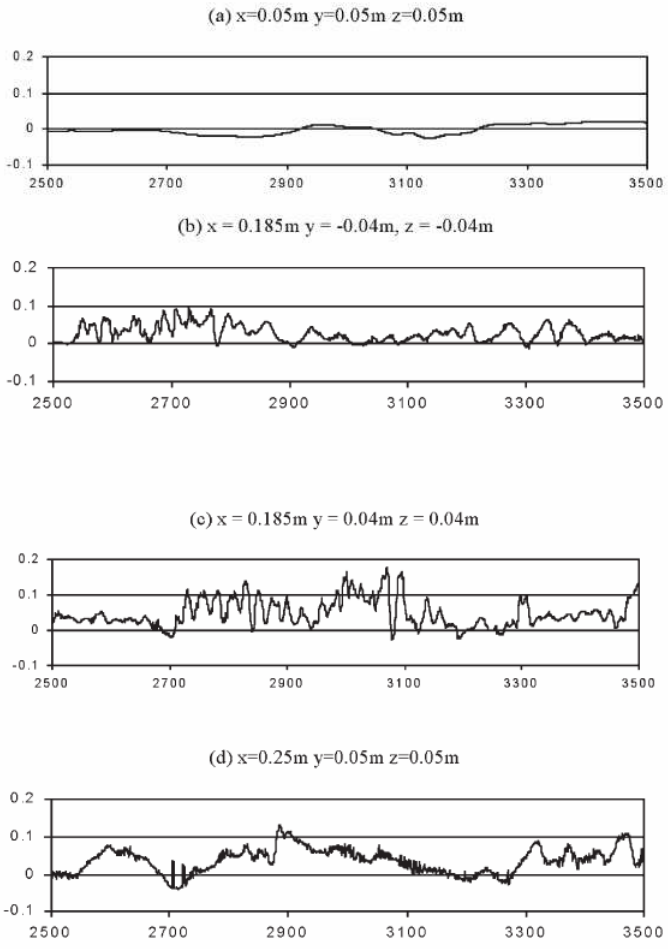

Figure 3. Time series plots of axial velocity for the PBT from 168.13306 (2500 time steps) to 178.12756 s (3500 time steps) after start-up from a zero-velocity field.

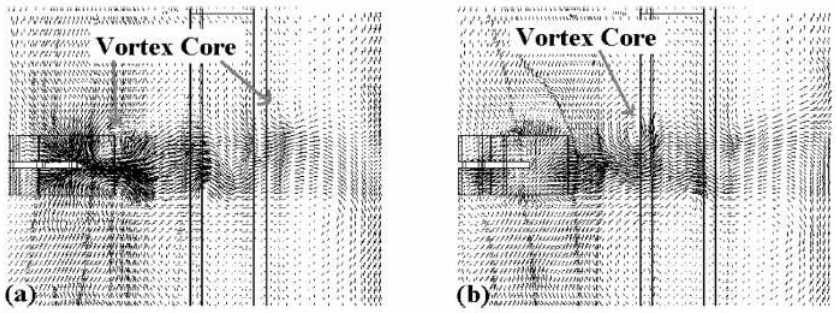

Figure 4. The unsteady flow created by a Rushton turbine.

which are located just below the impeller blade tip, than in locations (d), close to the vessel bottom, and (a), which is close to the liquid surface.

Instantaneous Flow Field for the Rushton Turbine

Figure 4 shows the unsteady flow field in the outflow of the Rushton turbine, at two instances in time separated by 0.024 s, which corresponds to 0.7 of a blade passage period. Figure 4a shows the trailing vortex forming just behind the impeller blade on the left. The vortex core indicated on the right in Figure 4a is the core of the trailing vortex behind the previous blade. Figure 4b shows how the vortex core coming from the blade has moved radially outwards. These results qualitatively agree with the results reported by Eggels (1996) and Derksen and Van den Akker (1999).

Figure 5 shows the vortices behind the impeller blades by means of an iso-surface of constant vorticity magnitude ($550\ s^{-1}$) coloured by velocity magnitude. The flow direction at the vessel wall and bottom is also shown, by means of so-called oilflow lines. Oilflow lines are pathlines that are constrained to the surface from which the flow-following particles are released. The colour of the oilflow lines also denotes the velocity magnitude. The vortices behind the impeller blades are clearly visible. The vortices attach on one end to the impeller disk and follow the outline of the blade, separating from the blade at the blade tip.

Figure 6 shows a snapshot of the overall turbulent flow structure in the vessel. An iso-surface of vorticity magnitude ($80\ s^{-1}$) is shown, again coloured by velocity magnitude. The large number of turbulent flow structures is apparent. It should be noted that the flow field is unsteady, and that Figures 5 and 6 show snapshots of the flow field only. For example, the vortices near the shaft are highly unsteady, and vortices continually form, move, and decay in an unsteady fashion.

Instantaneous Flow Field for the HE-3 Impeller

Figure 7 shows an instantaneous flow field result for the HE-3 impeller. The flow is shown by means of oilflow lines at the liquid surface. Figure 8 shows the oilflow lines at the vessel wall at the same instant in time. The oilflow lines are coloured by velocity magnitude, with

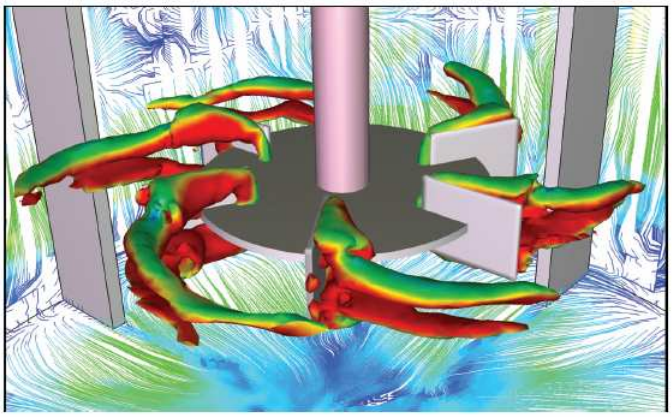

Figure 5. The vortices created behind the blades of a Rushton turbine, at one instant in time. The vortices are visualized by means of an iso-surface of vorticity magnitude ($550\ s^{-1}$), coloured by velocity magnitude. The flow direction at the vessel wall and bottom is shown by means of oilflow lines. Colour denotes the velocity magnitude in ($m\ s^{-1}$) using the same scale as Figure 6.

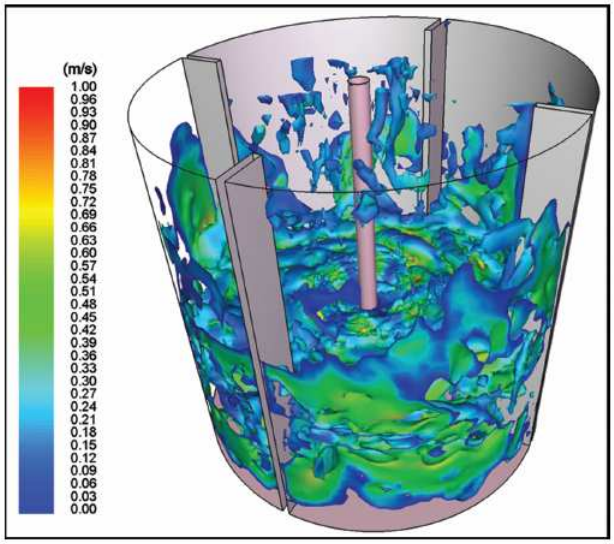

Figure 6. Turbulent structures in a stirred vessel equipped with a Rushton turbine are shown by means of iso-surfaces of vorticity magnitude (80 s^{-1}), coloured by velocity magnitude.

red denoting a high velocity and blue indicating a low velocity. The complex turbulent structures that form within the vessel are clearly visible. Vortices are also visible at the liquid surface.

Instantaneous Flow Field for the Multiple A310 Impeller System

Figure 9 shows instantaneous flow field results for the multiple A310 impeller system. The flow is shown by means of contour plots of velocity magnitude. The different outflow pattern for each of the four impellers is clearly visible. Obviously, these flow patterns are unstable, with the flow between the impellers periodically separating and reattaching.

Glass-Lined Mixing Equipment

Glass-lined equipment is typically used for applications that involve highly corrosive materials. The glass coating

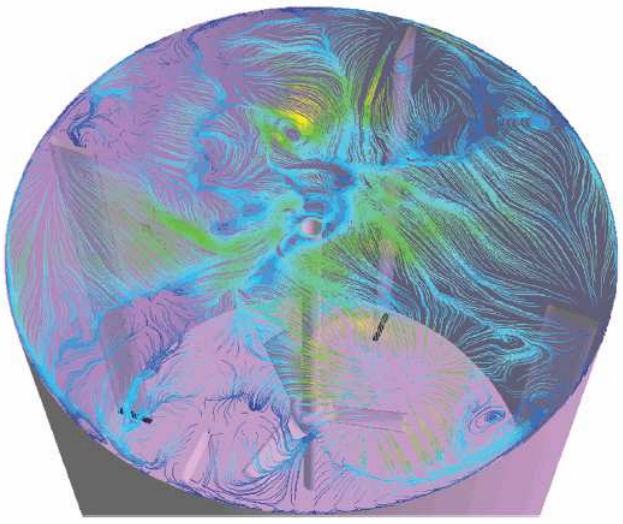

Figure 7. Oilflow lines at the liquid surface for an HE-3 impeller. The impeller rotates clockwise as seen from the top. The colour indicates the local velocity magnitude ranging from 0 m s^{-1} (dark blue) to 0.05 m s^{-1} (red).

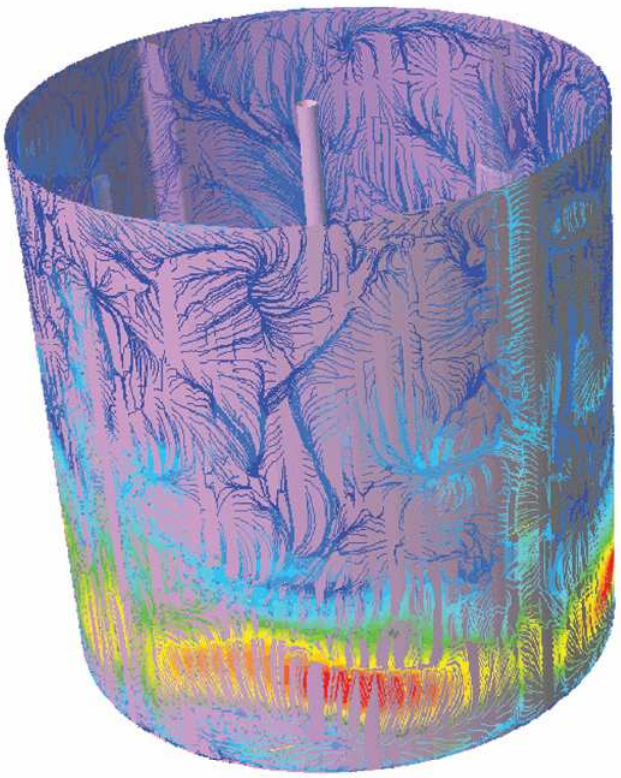

Figure 8. Oilflow lines at the vessel wall for an HE-3 impeller. The colour indicates the local velocity magnitude ranging from 0 m s^{-1} (dark blue) to 0.05 m s^{-1} (red).

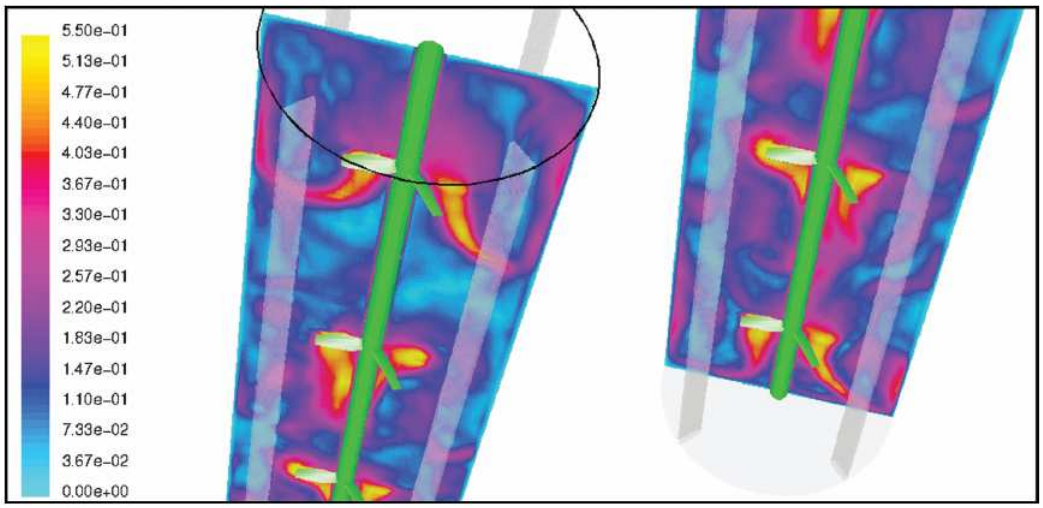

Figure 9. Instantaneous flow field result for the multiple A310 system. The colour denotes velocity magnitude in m s^{-1}.

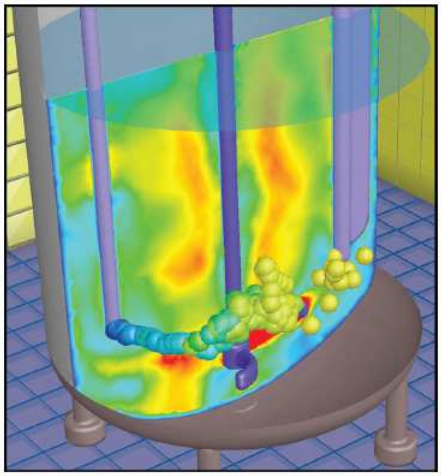

Figure 10. Dispersion in a glass-lined vessel equipped with a retreat curve impeller. The flow following particles are injected from the dip tube and dispersed from there. The centre plane is coloured by liquid velocity magnitude. The color scale is the same as in Figure 11.

is inert with respect to the chemical reaction, thus protecting the metal from the corrosive chemicals. The geometry of impellers, baffles, and vessels in glass-lined systems is restricted by the fact that there can be no sharp edges, to which the glass would not adhere, and by the fact that baffles have to be suspended from flanges in the top head. They cannot be welded or bolted to the vessel as is common in other applications. Thus the geometry of glass-lined mixing systems is typically very different from so-called 'alloy equipment'. Because of the reduced baffling in these systems, the degree of swirl is relatively high. This sometimes leads to vortices slowly precessing around the shaft (depending on the liquid level), a phenomenon that is well suited for analysis using LES.

Figure 10 shows the dispersion of flow following particles in a glass-lined vessel equipped with a retreat curve impeller. The particles are injected from the dip tube and dispersed from there. The centre plane is coloured by liquid velocity magnitude. Figure 11 shows the flow field at the liquid surface of this vessel as shown by oilflow lines. The colour denotes the local liquid velocity. The retreat curve impeller rotates counter-clockwise as seen from the top. Each consecutive image is taken 0.09 s

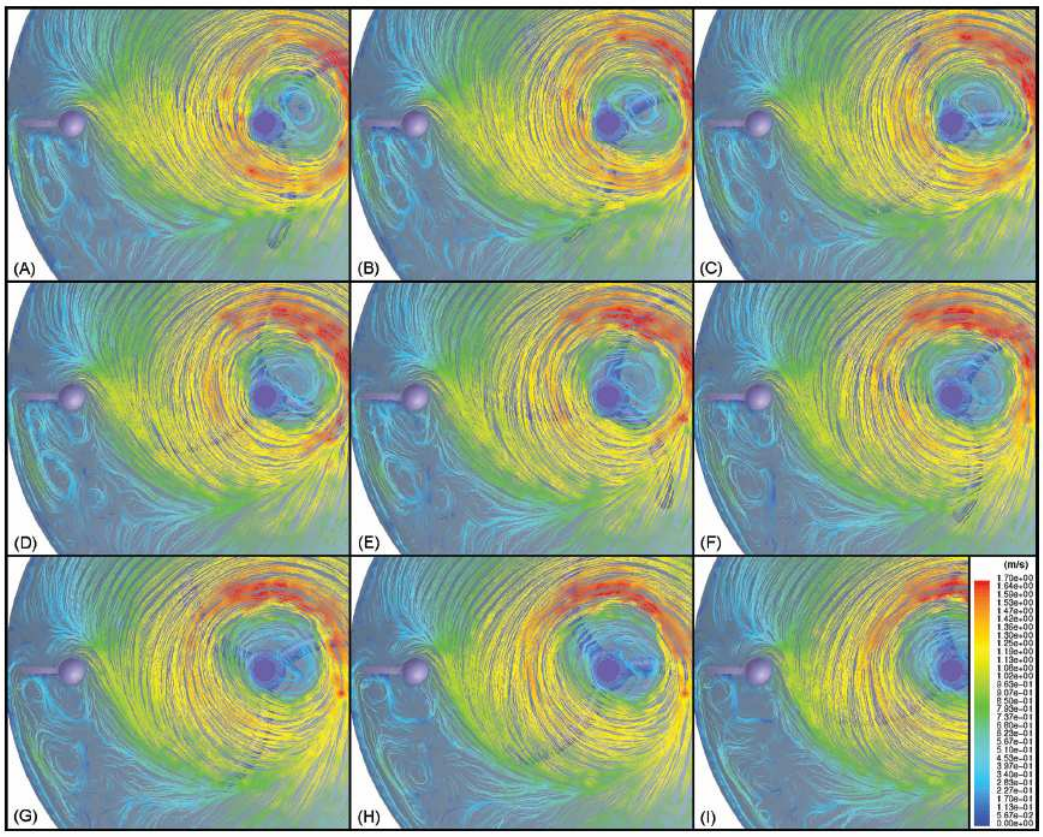

Figure 11. The flow field at the liquid surface of the glass-lined vessel as shown by oilflow lines at different instances in time. The colour denotes the local liquid velocity magnitude.

after the previous image, and the whole sequence covers 0.72 s (2.2 impeller revolutions). The surface vortex adjacent to the shaft (to the right of the shaft) stays in the same location during this time period. The vortex near the shaft precesses slowly around the shaft, and the current data were extrapolated to determine the precession period to be approximately once in every 40 impeller revolutions. The vortices behind the baffle (on the left side) move and shed at a frequency that is much closer to the impeller rotational frequency.

CONCLUSIONS

In this study, the application of large eddy simulation to the prediction of large-scale chaotic structures in stirred tanks was investigated. Flow regimes representing typical stirrer configurations were assessed. The predicted flow patterns for the PBT compared well with digital particle image velocimetry data reported in the literature, and exhibited the long time-scale instabilities seen in the experiments. The results for the Rushton turbine compared well with LES simulations reported previously.

The results clearly show the richness in structures that the turbulent flow fields in stirred tanks exhibit. Many different unsteady flow structures were observed, across a wide variety of flow regimes. Considering this, it is perhaps not surprising that a full understanding of the hydrodynamics of these flows has so far eluded researchers despite many years of research.

Many previously unexplained hydrodynamic phenomena that are observed in stirred vessels, such as the time-dependent settling of solids in dilute suspensions and large variations in measured blend times in seemingly identical experiments, can possibly be explained by the time-varying flow fields that were observed. However, much additional research is needed to come to a full understanding of these phenomena.

It should be noted that flow field calculations using LES are one to two orders more time consuming than RANS calculations. At present, LES is therefore most suited as an analysis tool, and still less suited for practical engineering design use.

NOMENCLATURE

C	distance from impeller to bottom, m
C	model constant
C_{rng}	model constant
C_{s}	model constant
d	distance to closest wall, m
D	impeller diameter, m
H	heaviside step function
L_{s}	mixing length, m
S	strain rate, s^{-1}
T	vessel diameter, m
u_i	velocity in i direction, $\mathrm{m\,s}^{-1}$
V	cell volume, m^3
W	impeller blade width, m
W_{b}	baffle blade width, m
x	x-coordinate, m
x_i	spatial coordinate in direction i, m
y	y-coordinate, m
z	z-coordinate, m
Z	liquid level, m

Greek symbols

δ_{ij}	Kronecker delta
κ	model constant
μ	molecular viscosity, $\mathrm{kg\,m}^{-1}\,\mathrm{s}^{-1}$
μ_{eff}	effective viscosity, $\mathrm{kg\,m}^{-1}\,\mathrm{s}^{-1}$
μ_{sgs}	subgrid scale viscosity, $\mathrm{kg\,m}^{-1}\,\mathrm{s}^{-1}$
μ_{t}	turbulent viscosity, $\mathrm{kg\,m}^{-1}\,\mathrm{s}^{-1}$
ρ	density, $\mathrm{kg\,m}^{-3}$
σ_{ij}	subgrid scale stresses, Pa
τ	shear stress, Pa

REFERENCES

Bakker, A., Oshinowo, L.M. and Marshall, E.M., 2000, The use of large eddy simulation to study stirred vessel hydrodynamics. Proceedings of the 10th European Conference on Mixing, Delft, The Netherlands, July 2–5, 2000, pp 247–254.

Bakker, A., Haidari, A. and Marshall, E.M., 2001, Modeling stirred vessel hydrodynamics using large eddy simulation. Presented at Mixing XVIII, June 24–29, 2001, Pocono Manor, Pennsylvania, USA.

Bakker, A., Dhanasekharan, K., Haidari, H. and Kim, S.E., 2002, Modeling of turbulence in stirred vessels using large eddy simulation. Presented at CHISA 2002, August 25–29, 2002, Prague, Czech Republic.

Bakker, A., LaRoche, R.D., Wang, M.H. and Calabrese, R.V., 1997, Sliding mesh simulation of laminar flow in stirred reactors, *Trans IChemE, Part A, Chem Eng Res Des*, 75: 42–44.

Bakker, A. and Van den Akker, H.E.A., 1994a, Single-phase flow in stirred reactors, *Trans IChemE, Part A, Chem Eng Res Des*, 72: 583–593.

Bakker, A. and Van den Akker, H.E.A., 1994b, Gas–liquid contacting with axial flow impellers, *Trans IChemE*, Part A, Chem Eng Res Des, 72: 573–582.

Derksen, J. and Van den Akker, H.E.A., 1999, Large eddy simulations on the flow driven by a Rushton turbine, *AIChE J*, 45: 209–221.

Eggels, J.G.M., 1996, Direct and large-eddy simulations of turbulent fluid flow using the lattice–Boltzmann scheme, *Int J Heat Fluid Flow*, 17: 307.

Hartmann, H., Derksen, J.J. and Van den Akker, H.E.A., 2003, An LES investigation of the flow macro-instability in a Rushton turbine stirred tank. Proceedings of the 11th European Conference on Mixing, Bamberg, Germany, 14–17 October 2003, pp 285–292.

Lilly, D.K., 1966, On the application of the eddy viscosity concept in the inertial subrange of turbulence. NCAR Manuscript 123.

Mathur, S.R., 1994, *Unsteady flow simulations using unstructured sliding meshes*, AIAA 25th Fluid Dynamics Conference, June 20–23, 1994, Colorado Springs, CO.

Murthy, J.Y. and Mathur, S.R., 1998, A finite volume method for radiative heat transfer using unstructured meshes. AIAA-98-0860, January 1998.

Myers, K.J., Ward, R.W. and Bakker, A., 1997, A digital particle image velocimetry investigation of flow field instabilities of axial flow impellers, *J Fluids Engng, Trans ASME*, 119: 623–632.

Roussinova, V.T., 2001, Low frequency macroinstabilities in a stirred tank. MSc thesis, Fall 2001, Department of Chemical and Material Engineering, University of Alberta, Edmonton, Alberta, Canada.

Smagorinsky, J., 1963, General circulation experiments with the primitive equations, I. The basic experiment, *Month Wea Rev*, 91: 99–164.

Yakhot, A., Orszag, S.A., Yakhot, V. and Israeli, M., 1986, Renormalization group formulation of large-eddy simulation, *J Sci Comput*, 1: 1–51.

Yeoh, S.L., Papadakis, G. and Lee, K.C. (2003) Large eddy simulation of turbulent flow in Rushton impeller stirred reactor with a sliding-deforming mesh methodology. Proceedings of the 11th European Conference on Mixing, Bamberg, Germany, 14–17 October 2003, pp 39–46.

ACKNOWLEDGEMENTS

The authors wish to thank Elizabeth M. Marshall, Ahmad Haidari, Kumar Dhanasekharan, and Sung-Eun Kim for their contributions.

The manuscript was received 29 March 2004 and accepted for publication after revision 15 July 2004.